Cellular/Molecular

Congenital Stationary Night Blindness Type 2 Mutations S229P, G369D, L1068P, and W1440X Alter Channel Gating or Functional Expression of $Ca_v1.4$ L-type Ca^{2+} Channels

Jean-Charles Hoda,[1] **Francesca Zaghetto,**[1,2] **Alexandra Koschak,**[1] **and Jörg Striessnig**[1]

[1]Abteilung Pharmakologie und Toxikologie, Institut für Pharmazie, Universität Innsbruck, A-6020 Innsbruck, Austria, and [2]Dipartimento di Farmacologia e Anestesiologia, Università Degli Studi Di Padova, 35131 Padova, Italy

Mutations in the *CACNA1F* gene (voltage-dependent L-type calcium channel $\alpha1F$ subunit) encoding retinal $Ca_v1.4$ L-type Ca^{2+} channels cause X-linked recessive congenital stationary night blindness type 2 (CSNB2). Many of them are predicted to yield nonfunctional channels. Complete loss of $Ca_v1.4$ function is therefore regarded as a pathogenetic mechanism for the impaired signaling from photoreceptors to second-order retinal neurons. We investigated the functional consequences of CSNB2 missense mutations S229P, G369D, and L1068P and the C-terminal truncation mutant W1440X.

After expression in *Xenopus laevis* oocytes or human embryonic kidney tsA-201 cells, inward Ca^{2+} current (I_{Ca}) and inward Ba^{2+} current (I_{Ba}) could be recorded from mutations G369D and L1068P. G369D shifted the half-maximal voltage for channel activation ($V_{0.5,act}$) significantly to more negative potentials (>11 mV), slowed inactivation, and removed Ca^{2+}-dependent inactivation. The L1068P mutant yielded currents only in the presence of the channel activator BayK8644. Currents (I_{Ba}) inactivated faster than wild type (WT) and recovered more slowly from inactivation (I_{Ba} and I_{Ca}). No channel activity could be measured for mutants S229P and W1440X after oocyte expression. No W1440X $\alpha1$ protein was detected after expression in tsA-201 cells, whereas S229P (as well as G369D and L1068P) $\alpha1$ subunits were expressed at levels indistinguishable from WT ($n = 3$).

Our data provide unequivocal evidence that CSNB2 missense mutations can induce severe changes in $Ca_v1.4$ function, which may decrease (L1068P and S229P) or even increase (G369D) channel activity. The lower activation range of G369D can explain the reduced dynamic range of photoreceptor signaling. Moreover, we demonstrate that loss of channel function of one (L1068P) CSNB2 mutation can be rescued by a Ca^{2+} channel activator.

Key words: voltage-gated Ca^{2+} channels; congenital stationary night blindness; missense mutations; genetic diseases; sensory cells; channelopathies

Introduction

Different types of voltage-gated Ca^{2+} channels mediate depolarization-induced Ca^{2+} entry into electrically excitable cells (Catterall, 2000). Ca_v2 Ca^{2+} channels targeted to the neurotransmitter release sites at nerve terminals (Zamponi, 2003) control fast (phasic) neurotransmitter release in neurons (Wheeler et al., 1994). In contrast, Ca_v1 L-type Ca^{2+} channels (LTCCs) mediate tonic neurotransmitter release in sensory cells such as cochlear inner hair cells and the retina. In cochlear inner hair cells, L-type currents are formed exclusively by $Ca_v1.3$ (Platzer et al., 2000). In photoreceptors and bipolar cells, $Ca_v1.3$ and $Ca_v1.4$ exist (Morgans et al., 2001; Ball et al., 2002; Barnes and

Kelly, 2002; McRory et al., 2004), but their relative contribution to total Ca^{2+} influx and the visual process remains unclear. Photoreceptors depolarize from a resting potential of approximately -55 mV during a light stimulus (Witkovsky et al., 1997) to approximately -40 mV in the dark, thus eliciting depolarization-induced Ca^{2+} influx through LTCCs (Corey et al., 1984; Witkovsky et al., 1997; Schneeweis and Schnapf, 2000; Moriondo et al., 2001). This triggers tonic glutamate release from the photoreceptor terminals (Morgans, 2000). $Ca_v1.3$ and $Ca_v1.4$ LTCCs are especially suited for supporting tonic Ca^{2+} influx, because they inactivate incompletely during maintained depolarizations and activate quickly at voltages below -40 mV (Koschak et al., 2003; Baumann et al., 2004; McRory et al., 2004).

$Ca_v1.4$ $\alpha1$ subunits predominantly occur in retinal neurons but were also detected in dorsal root ganglia (Murakami et al., 2001), lymphatic organs, and immune cells (McRory et al., 2004). Their contribution to retinal function is evident from mutations in the $Ca_v1.4$ gene [*CACNA1F* (voltage-dependent L-type calcium channel $\alpha1F$ subunit)], which cause X-linked congenital stationary night blindness type 2 (CSNB2) (Bech-Hansen et al., 1998; Strom et al., 1998). The term is misleading, because night

blindness may not be the major complaint. Typical CSNB2 symptoms are moderately low visual acuity, myopia, nystagmus, and variable levels of night blindness, but one or more of these symptoms may be absent (Boycott et al., 2000). The eye fundus is normal, but electroretinograms are severely abnormal, with changes indicating a defect in neurotransmission between photoreceptors and second-order neurons (Tremblay et al., 1995).

Most of the >40 structural *CACNA1F* aberrations cause severe structural changes, such as truncated α1 subunits, unlikely to support significant channel activity. In the absence of a functional allele in affected males, this implies that CSNB2 can result from a complete loss of Ca$_v$1.4 channel function. This is in contrast to a recent finding that some single missense mutations do not alter channel function after expression in mammalian cells (McRory et al., 2004).

In this study, we present a detailed biophysical analysis of three CSNB2 missense mutations and a C-terminal truncation mutant. Our data provide convincing evidence that all of them result in profound changes of Ca$_v$1.4 channel gating or functional channel expression. We also show that CSNB2 mutations can lead to increased LTCC function, suggesting that both gain and loss of LTCC function must be able to hamper photoreceptor signaling to second-order retinal neurons.

Materials and Methods

Ca$_v$1.4 cDNA mutants
Mutations were introduced into the Ca$_v$1.4 α1 cDNA (Strom et al., 1998) cloned previously from human retina (Koschak et al., 2003) (GenBank accession number NM_005153; open reading frame length, 5898 bp). Nucleotide positions of endonuclease restriction sites are given in parentheses.

Mutants were constructed by applying the "geneSOEing" technique (Horton et al., 1989). For heterologous expression in *Xenopus laevis* oocytes, Ca$_v$1.4 cDNA together with the polyadenylation sequence of pNKS2 plasmid (a gift from O. Pongs, ZMNH, Hamburg, Germany) was cloned into the *Nhe*I–*Xba*I polylinker sites of the expression vector pCIneo by coligating Ca$_v$1.4 cDNA (*Nhe*I–*Sma*I) and the polyadenylation sequence (*Sma*I–*Xba*I).

Mutants S229P (SP) and G369D (GD) were constructed by using an *Nhe*I–*Age*I (−12–1390) cassette subsequently ligated into the *Nhe*I–*Age*I (−12–1390)-cut Ca$_v$1.4 α1–pCIneo construct. Mutant L1068P (LP) was cloned using a *Bst*1107I–*Eco*RI (3105–4348) cassette, respectively.

For the construction of the truncated mutant W1440X (WX), a termination codon was introduced by PCR. The *Age*I–*Eco*RI-cut PCR fragment was ligated into the *Age*I–*Eco*RI (1390–4348)-cut Ca$_v$1.4 α1–pCIneo cDNA. The integrity of all of the constructs was confirmed by DNA sequencing (MWG Biotech, Ebersberg, Germany).

Transient expression of Ca$_v$1.4 mutants in mammalian cells
For patch-clamp recordings, human embryonic kidney tsA-201 cells were transfected with human Ca$_v$1.4 wild-type (WT) α1, mutant GD, or mutant LP α1 subunit cDNA together with β3 (Castellano et al., 1993) and α2δ1 (Ellis et al., 1988) auxiliary subunits, as described previously in our first characterization of Ca$_v$1.4 (Koschak et al., 2003). For immunoblotting, membranes from tsA-201 cells transfected with 3 μg of α1, 2 μg of β3, and 2.5 μg of α2δ1 subunit cDNA, and 2.5 μg of pUC18 carrier DNA in 10 cm culture dishes were prepared as described previously (Huber et al., 2000). Immunoblotting was performed as described previously using a generic anti-α1 sequence-directed antibody (raised against a synthetic peptide corresponding to residues 1382–1400 of the Ca$_v$1.1 α1 subunit) (Safayhi et al., 1997).

Expression of Ca$_v$1.4 mutants in X. laevis oocytes
Capped runoff poly(A$^+$) cRNA transcripts from *Xba*I-linearized cDNA templates were synthesized according to the protocol of Krieg and Melton (1984) (using T7 polymerase). cRNA encoding wild-type or mutant Ca$_v$1.4 α1 subunits were mixed at equimolar concentrations with auxil-

iary subunits β2a (Perez-Reyes et al., 1992) or β3 (Castellano et al., 1993) and α2δ1 (Ellis et al., 1988). Fifty nanoliters of this cRNA mixture (0.1–0.33 pmol/μl) was injected using a Microdispenser (Drummond Scientific, Bromall, PA) into freshly isolated and defolliculated stages V and VI *X. laevis* oocytes. Currents were measured 4–7 d after injection. Microinjected oocytes were kept at 19°C in a sterile ND96 medium (in mM: 96 NaCl, 2 KCl, 1 MgCl$_2$, 5 HEPES, and 1.8 CaCl$_2$, adjusted to pH 7.5 with NaOH) and supplemented with 100 U/ml penicillin and 100 μg/ml streptomycin (Sigma, St. Louis, MO).

Electrophysiological recordings
X. laevis oocytes. Four to 7 d after cRNA injection, inward Ba^{2+} current (I_{Ba}) or inward Ca^{2+} current (I_{Ca}) was measured at 21–23°C by a two-microelectrode voltage clamp using an oocyte clamp NPI Electronic (Tamm, Germany) amplifier connected through an Axon Instruments (Union City, CA) digidata 1322A analog-to-digital board and interfaced to a personal computer.

Before recording I_{Ba} or I_{Ca}, oocytes were injected with 30 nl of 100 mM BAPTA solution, pH 7.4, to prevent contamination by Ca^{2+}-activated Cl$^-$ and K$^+$ conductances. To exclude the possibility that the slowly inactivating Ca$_v$1.4 currents were contaminated by Ca^{2+}- or Ba^{2+}-activated Cl$^-$ currents despite injection of BAPTA, we tested the effect of 70 mM extracellular chloride, which must result in Cl$^-$ inward currents mimicking faster LTCC inactivation. Such changes were present without intracellular Ca^{2+} buffering but were not observed after BAPTA injection for BayK8644 (BayK)-stimulated Ca$_v$1.4 ($n > 4$) or slowly inactivating Ca$_v$1.2 currents (coexpressed with β2a and α2δ1; $n > 8$; data not shown). Similarly, no evidence for contamination by (inward) K$^+$ current was observed after inclusion of 100 mM K$^+$ in the bath ($n > 4$; data not shown).

As a control, endogenous I_{Ba} was measured from oocytes injected only with β3 and α2δ1 auxiliary subunits. I_{Ba} and I_{Ca} were recorded only from oocytes in which I_{Ba} and I_{Ca} exceeded the highest endogenous currents in the same oocyte batch by at least fourfold to fivefold (0.25 nA). Currents larger than 1.2 μA were not included in the analysis. Data analysis and acquisition were performed by using the pClamp software package (version 9.0; Axon Instruments). Microelectrodes were filled with 2.8 M CsCl, 0.2 M CsOH, 10 mM EGTA, and 10 mM HEPES, adjusted to pH 7.4 with HCl, and had resistances of 0.1–1.2 MΩ.

During I_{Ba} recordings, oocytes were perfused with a solution containing the following (in mM): 10 Ba(OH)$_2$, 50 Na(OH), 2 CsOH, and 5 HEPES, adjusted to pH 7.4 with methanesulfonic acid. To obtain I_{Ca}, the bath solution was switched to a solution containing Ca(NO$_3$)$_2$ instead of Ba(OH)$_2$.

Leak correction was performed by adjusting the current traces by a factor calculated from the difference between the leak at −80 and −90 mV, respectively. Voltage dependence of activation was determined from I–V curves obtained by step depolarizations from a holding potential of −80 mV to different test potentials. The half-maximal voltage for channel activation ($V_{0.5,act}$), the slope factor of the curve at $V_{0.5,act}$ (k_{act}), the maximal slope conductance (G), and the reversal potential were obtained by fitting the data to the Boltzmann equation (Koschak et al., 2003).

Inactivation was determined by applying a 10 sec depolarizing pulse from a holding potential of −80 mV to a test potential 10 mV positive to the maximum of the current–voltage relationship (V_{max}) estimated from the I–V relationship.

Recovery from inactivation was studied using a multipulse protocol. After a 10 sec depolarizing pulse to V_{max} plus 10 mV from a holding potential of −80 mV, the time course of I_{Ba} recovery was determined by applying 50 msec test pulses to the same potential at 0.5, 1, 2, 5, and 10 sec after the prepulse.

tsA-201 cells. Whole-cell patch-clamp experiments were performed as described by us previously (Koschak et al., 2003) using 15 mM Ba^{2+} as a charge carrier.

Statistical analysis
Data were analyzed using the pClamp software package (version 9.0; Axon Instruments). Origin (OriginLab, Northampton, MA) and Graph-

Pad Prism 4 software (GraphPad Software, San Diego, CA) were used for nonlinear curve fitting and statistical data analysis. All data are given as means ± SE for the indicated number of experiments. Statistical significance was determined by unpaired Student's t test and one-way ANOVA, followed by the Bonferroni multiple-comparison test as indicated.

Results

We introduced three CSNB2 missense mutations, SP, GD, and LP, into Ca$_v$1.4 α1 subunits. As illustrated in Figure 1, mutation GD is located at the end of IS6, LP in the pore-forming S5–S6 linker of repeat III, and SP within the IS4–IS5 linker (Fig. 1). SP aligns with residue S218 of Ca$_v$2.1 channels, which has been found to cause a severe form of familial hemiplegic migraine type 1 (FHM1) (with delayed cerebral edema and coma after minor head trauma) (Kors et al., 2001). We also constructed mutation WX, which causes a truncation of most of the C-terminal tail (Fig. 1). All of these mutations concern highly conserved amino acids, as shown in sequence alignments with other L-type and non-L-type (Ca$_v$2.1) Ca^{2+} channels in Figure 1.

We have shown recently that only a small fraction (22%) of tsA-201 cells successfully transfected with Ca$_v$1.4 Ca^{2+} channels also express measurable currents (Koschak et al., 2003). This low-expression yield complicated a detailed electrophysiological analysis in this expression system. For routine analysis of channel mutants, we therefore expressed Ca$_v$1.4 channels in *X. laevis* oocytes, which gave robust expression 3–6 d after cRNA injection. Because previous studies have shown that Ca$_v$1.4 current-gating properties are only minimally affected by β subunit isoforms (Koschak et al., 2003; McRory et al., 2004), we coexpressed Ca$_v$1.4 α1 together with α2δ1 and β3 subunits, which resulted in higher currents than α2δ1 plus β2a in *X. laevis* oocytes ($n = 20$; data not shown). To further increase current amplitudes (especially smaller I_{Ca}; see below), most recordings were performed in the presence of 10 μM BayK, but data without BayK were also obtained when appropriate.

In oocytes, WT channels mediated I_{Ba} with characteristics very similar to tsA-201 cell-expressed currents (Koschak et al., 2003; Baumann et al., 2004; McRory et al., 2004). With 10 mM Ba^{2+} as charge carrier, $V_{0.5,act}$ was −12.8 and −17.7 mV in the absence and presence of 10 μM BayK, respectively ($n = 20$–35) (Table 1; Fig. 2A,B). During a 10 sec depolarization to the maximum of the I–V curve, 36.6 ± 0.84% ($n = 23$) of I_{Ba} was inactivated (Fig. 3A–D). When Ba^{2+} was replaced by Ca^{2+} as the charge carrier, the fraction of current inactivating during a 10 sec pulse increased significantly (51.8 ± 1.46%; $n = 19$; $p < 0.001$), indicating the presence of Ca^{2+}-dependent inactivation (CDI) under our experimental conditions (Fig. 3A–D). Because CDI is absent under conditions of strong intracellular Ca^{2+} buffering (Koschak et al., 2003) in tsA-201 cells, it is possible that Ca^{2+} buffering at the cytoplasmic side of the channel is weaker in oocytes despite injection of 30 nl of 100 mM BAPTA (see Materials and Methods). This would permit a form of CDI that can only occur with weak intracellular Ca^{2+} buffering as observed, for
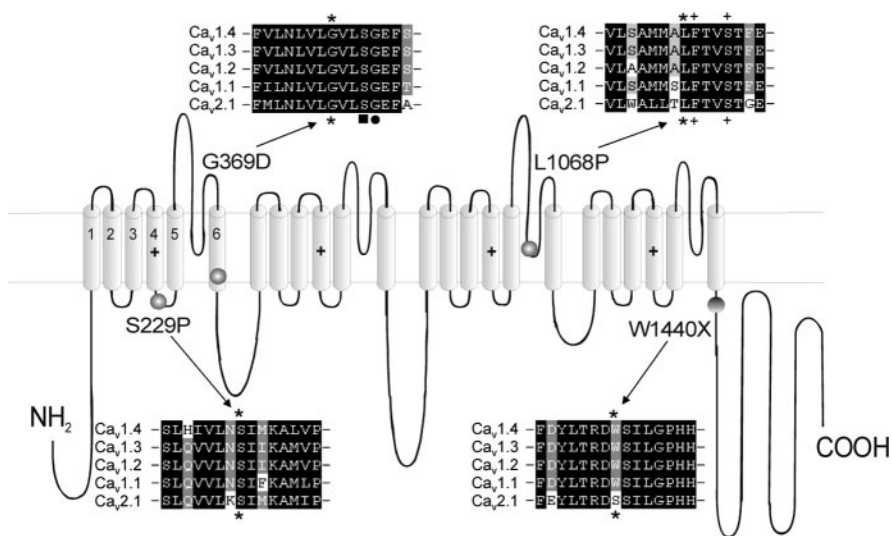

Figure 1. Location of missense mutations SP, GD, LP and truncated mutation WX in the Ca$_v$1.4 α1 subunit. For each mutation, a corresponding ClustalW sequence alignment between human Ca$_v$1.4 α1, DHP-sensitive Ca$_v$1.3 α1, Ca$_v$1.2 α1, Ca$_v$1.1 α1, and DHP-insensitive Ca$_v$2.1 α1 (NCBI GenBank accession numbers NM_005183, NM_000720, NM_000719, NM_000069, and NM_023035, respectively) was performed in a small region seven amino acids before and after the mutation. All of the amino acids mutated in Ca$_v$1.4 α1 subunit (indicated by asterisks) were highly conserved among L-type and non-L-type Ca^{2+} channels (as shown for Ca$_v$2.1 α1). In the alignment of mutant LP, two amino acids critical for DHP agonist binding are indicated by + (Yamaguchi et al., 2003). In the alignment of mutant GD, the black square indicates a serine residue important for slow inactivation in IS6 (Shi and Soldatov, 2002), and the black dot indicates the recently found Ca$_v$1.2 G406R missense mutation responsible for Timothy syndrome (Splawski et al., 2004).

example, for Ca$_v$2.1 (P- and Q-type channels) (Liang et al., 2003). We therefore used Ca$_v$2.1 to test our hypothesis. Replacement of Ba^{2+} by Ca^{2+} in the perfusing solution significantly increased the inactivation of Ca$_v$2.1 currents from 39.8 ± 1.4 to 82.3 ± 3.8% ($n = 4$) during 10 sec pulses to V_{max}. The possibility that the slowly inactivating Ca$_v$1.4 currents were contaminated by Ca^{2+}- or Ba^{2+}-activated Cl$^-$ or K$^+$ currents despite intracellular BAPTA injection could be excluded in experiments with 70 mM Cl$^-$ or 100 mM K$^+$ in the bath (see Materials and Methods). Thus, the CDI behavior of Ca$_v$1.4 resembles more closely the calmodulin N-lobe-mediated CDI of non-LTCCs rather than the calmodulin C-lobe-mediated CDI of LTCCs (Koschak et al., 2003; Liang et al., 2003; McRory et al., 2004).

Subsequently, we investigated whether mutants SP, GD, LP, and WX form functional channels in *X. laevis* oocytes. Mutant GD supported I_{Ba} and I_{Ca} with amplitudes comparable with WT in both the absence and presence of 10 μM BayK (Fig. 2, Table 1). In contrast, mutant LP never yielded I_{Ba} exceeding the endogenous current (Fig. 2C), but large currents were obtained after perfusing the same oocyte with 10 μM BayK (Fig. 2C). Mutants SP and WX did not mediate I_{Ba}, exceeding endogenous currents in six (SP) and four (WX) different pools of oocytes injected with different amounts of cRNA and recordings up to 7 d after injection.

Mutation GD caused profound changes in Ca$_v$1.4 channel characteristics. It significantly shifted the $V_{0.5,act}$ of I_{Ba} to more negative potentials by >13 mV in the absence and presence of BayK (Fig. 2A; Table 1). This shift was even larger for I_{Ca} (>20 mV) (Fig. 2B; Table 1) and remained when subgroups with different current amplitudes (0.30–0.59 vs 0.60–1.0 μA) were analyzed (data not shown). The GD mutation increased the time-to-peak current (Fig. 3A, inset) and strongly reduced current inactivation during 10 sec depolarizing pulses to V_{max} for both I_{Ba}

Table 1. Biophysical properties of Ca$_v$1.4 WT and CSNB2 mutations

	WT	GD	LP
$V_{0.5act}$ (mV)			
10 mM Ba^{2+}	-12.8 ± 0.5; $n = 20$	-26.5 ± 1.0***; $n = 16$	ND
10 mM Ba^{2+} + BayK	-17.7 ± 0.5; $n = 35$	-35.4 ± 1.0***; $n = 14$	-18.6 ± 0.5; $n = 12$
10 mM Ca^{2+} + BayK	-10.3 ± 0.5; $n = 30$	-31.8 ± 1.1***; $n = 8$	-15.1 ± 0.8***; $n = 15$
Activation threshold (mV)			
10 mM Ba^{2+}	-24.6 ± 0.4; $n = 20$	-39.4 ± 1.0***; $n = 16$	ND
10 mM Ba^{2+} + BayK	-28.7 ± 0.5; $n = 35$	-45.9 ± 1.2***; $n = 14$	-28.6 ± 0.4; $n = 12$
10 mM Ca^{2+} + BayK	-24.0 ± 0.5; $n = 30$	-43.2 ± 1.3***; $n = 8$	-27.5 ± 0.7***; $n = 15$
k_{act}			
10 mM Ba^{2+}	-4.7 ± 0.1; $n = 20$	-4.7 ± 0.2; $n = 16$	ND
10 mM Ba^{2+} + BayK	-3.9 ± 0.1; $n = 35$	-4.2 ± 0.3; $n = 14$	-3.8 ± 0.2; $n = 12$
10 mM Ca^{2+} + BayK	-5.0 ± 0.2; $n = 30$	-4.0 ± 0.2**; $n = 8$	-4.3 ± 0.2*; $n = 15$
Reversal potential (mV)			
10 mM Ba^{2+}	50.6 ± 0.5; $n = 20$	44.7 ± 0.9***; $n = 16$	ND
10 mM Ba^{2+} + BayK	46.9 ± 0.4; $n = 35$	44.4 ± 1.3*; $n = 14$	46.4 ± 0.9; $n = 12$
10 mM Ca^{2+} + BayK	53.6 ± 1.3; $n = 30$	45.3 ± 1.1**; $n = 8$	52.6 ± 1.5; $n = 15$
I_{Ba} versus I_{ca}			
G_{Ba} (mS)	12.7 ± 0.7; $n = 35$	10.0 ± 1.3; $n = 14$	11.1 ± 1.2; $n = 12$
G_{Ca} (mS)	11.1 ± 0.8; $n = 30$	11.0 ± 1.4; $n = 8$	13.0 ± 1.2; $n = 15$
Percentage change (same oocyte)	35.7 ± 2.8; $n = 24$	-33.9 ± 8.9***; $n = 6$	8.8 ± 5.9***; $n = 7$

Ca$_v$1.4 α1 WT and mutants GD and LP were coexpressed with β3 and α2δ1 subunits in *X. laevis* oocytes, and their activation properties were determined using 10 mM Ba^{2+} or Ca^{2+} as charge carrier. $V_{0.5,act}$, k_{act}, the reversal potential, and G (maximal slope conductance) were obtained by fitting the data to the Boltzmann equation, as described in Materials and Methods. The activation threshold was determined as the test potential at which 5% of the maximal current was activated. Data are given as mean $\pm$ SE; ND, not determined. Note that the shift in $V_{0.5,act}$ of GD and LP compared with WT could not be explained by currents with different amplitudes, because the differences persisted when smaller (0.25–0.59 μA) or larger (0.6–1.1 μA) currents were analyzed separately (data not shown). BayK, 10 μM BayK present. Conductance was measured in the presence of 10 μM BayK. Statistical differences for $V_{0.5,act}$, k_{act}, activation thresholds, reversal potentials, and G were calculated by one-way ANOVA, followed by the Bonferroni multiple-comparison test or by Student's t test when appropriate. *$p < 0.05$, **$p < 0.01$, ***$p < 0.001$ versus WT.
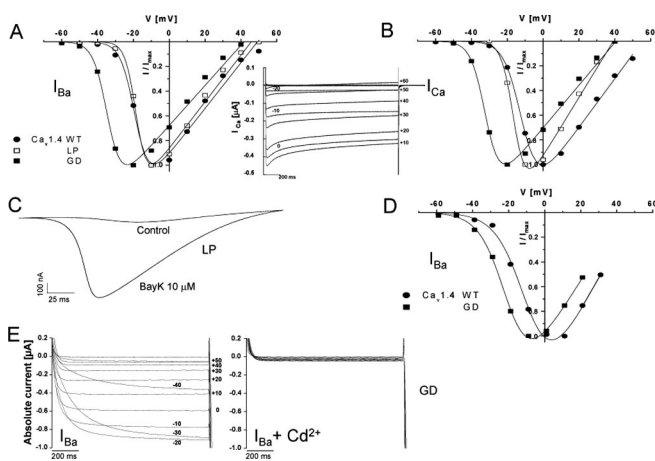

Figure 2. Activation properties of Ca$_v$1.4 WT and mutant α1 subunits. *A, B*, Normalized *I–V* curves for Ca$_v$1.4 WT and mutants GD and LP α1 subunits coexpressed with β3 and α2δ1 subunits in *X. laevis* oocytes. Ba^{2+} (*A*) or Ca^{2+} (*B*) were used as charge carriers with 10 μM BayK present in the bath. Representative *I–V* relationships are shown. For statistics, see Table 1. *B*, Inset, A representative original trace ($n > 3$) of Ca$_v$1.4 WT Ca^{2+} currents elicited by depolarizing pulses of 2 sec from -80 to $+60$ mV. *C*, Voltage ramps applied from a holding potential of -80 to $+70$ mV within 360 msec in the absence (control) and presence of 10 μM BayK in the same mutant LP-expressing oocyte. Such a BayK requirement for LP function was observed in all of the experiments ($n = 18$). A representative experiment is shown. *D*, Normalized *I–V* curves for Ca$_v$1.4 WT and mutant GD α1 subunits coexpressed with β3 and α2δ1 subunits in tsA-201 cells (as described in Materials and Methods) using 15 mM Ba^{2+} as charge carrier. Data points are means $\pm$ SE ($n = 40$ for WT and $n = 6$ for GD). *E*, Representative family of mutant GD Ba^{2+} currents elicited by 1 sec depolarizations from -80 to $+60$ mV before (left) and after (right) the addition of 1 mM Cd^{2+}, which resulted in a total block of the current.

(Fig. 3 *A, B*) and I_{Ca} (Fig. 3 *C, D*). After 10 sec, only $10.0 \pm 1.5\%$ of I_{Ba} ($n = 13$; $p < 0.001$ vs WT) and $8.2 \pm 0.87\%$ of I_{Ca} ($n = 12$; $p < 0.001$ vs WT) inactivated, indicating the absence of CDI in this mutant.

The GD mutation introduces a negative charge on the cytoplasmic end of IS6, which is involved in the formation of the

cytoplasmic end of the pore. Therefore, we investigated whether this mutation can alter the permeation properties of the channel. When switching from Ba^{2+}- to Ca^{2+}-containing solutions in the same oocyte, the maximal slope conductance (Table 1) for I_{Ca} through WT channels always decreased significantly by $33.5 \pm 4.3\%$ ($n = 12$). This indicates a lower permeability of the channel for Ca^{2+} than for Ba^{2+}, a typical property of L-type channels (Hess et al., 1986). In contrast to WT, the conductance for Ca^{2+} was always larger than for Ba^{2+} (increase by $33.9 \pm 8.9\%$; $n = 6$; $p < 0.001$ vs WT) in GD channels, suggesting a relative increase in the permeability of Ca^{2+} versus Ba^{2+}. The apparent reversal potential was significantly shifted to more negative voltages (Table 1), indicating a decrease in the divalent cation selectivity (Yang et al., 1993) of the GD channel. Cadmium completely blocked WT and mutant GD currents. No significant outward currents were observed at test potentials close to the reversal potential for I_{Ba} ($n > 3$ experiments for WT and GD) or I_{Ca} ($n > 2$ experiments for WT and GD) (Fig. 2 *E*).

The GD mutation was analyzed previously by McRory et al. (2004). They did not observe the same biophysical changes (see Discussion). We could rule out that the observed differences in $V_{0.5,act}$ of WT and GD were attributable to voltage errors introduced by different current amplitudes of mutant GD and WT (Table 1). To further confirm our findings obtained in oocytes, we also expressed GD in tsA-201 cells. Figures 2 *D* and 3, *E* and *F*, illustrate that similar biophysical changes were observed for GD channels in tsA-201 cells. As in oocytes, GD yielded maximal I_{Ba} amplitudes (I_{Ba} current density, 16.6 ± 6.0 pA/pF; $n = 6$) comparable with WT (21.3 ± 5.7; $n = 40$; 15 mM Ba^{2+}), shifted the activation of I_{Ba} by ~11 mV to more negative potentials (WT, $V_{0.5,act}$, -9.01 ± 0.76, $n = 40$; GD, $V_{0.5,act}$, -19.8 ± 1.8, $n = 6$; $p < 0.001$), increased the time-to-peak current (WT, 11.0 ± 3.5 msec, $n = 4$; GD, 365.1 ± 85.1 msec, $n = 6$; $p < 0.05$), and slowed inactivation of I_{Ba} during 10 sec depolarizations to V_{max} (WT, $68.6 \pm 2.4\%$, $n = 17$; GD, $46.5 \pm 8.1\%$, $n = 6$; $p < 0.01$).

For the LP mutant, significant current was only measurable in the presence of BayK in both *X. laevis* oocytes (Fig. 2 *C*) and
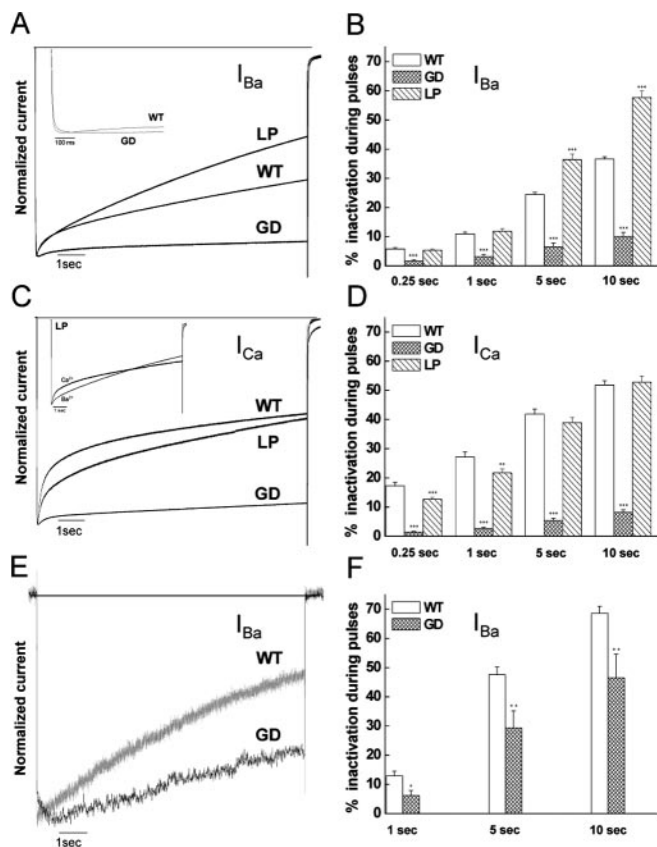
Figure 3. Inactivation properties of Ca$_v$1.4 WT and mutant α1 subunits. I_{Ba} (*A, B*) and I_{Ca} (*C, D*) through Ca$_v$1.4 WT and mutants GD and LP α1 subunits coexpressed with β3 and α2δ1 subunits in *X. laevis* oocytes were elicited by 10 sec depolarizing pulses from a holding potential of -80 mV to V_{max} plus 10 mV (10 μM BayK present). Traces were normalized to the peak current amplitudes. *A, C,* Representative current traces. *B, D,* Percentages of current inactivation were calculated after 0.25, 1, 5, and 10 sec depolarizations to the voltage of peak current plus 10 mV. Statistical differences for the percentage of inactivated current were determined by using one-way ANOVA, followed by the Bonferroni multiple-comparison test. Asterisks indicate statistically significant difference to WT (**$p < 0.01$; ***$p < 0.001$). GD increased the time-to-peak current (*A*, inset; WT, 19.5 $\pm$ 1.4 msec, $n = 23$; GD, 68.9 $\pm$ 13.3 msec, $n = 13$; $p < 0.001$). *B*, Inset, The complex inactivation time courses of I_{Ba} and I_{Ca} for mutant LP. *E, F,* I_{Ba} through Ca$_v$1.4 WT and mutant GD α1 subunits coexpressed with β3 and α2δ1 subunits in tsA201 cells were elicited by 10 sec depolarizing pulses from a holding potential of -90 mV to V_{max}. One representative experiment of six is shown. Currents were normalized to peak I_{Ba}. Percentages of current inactivation (*F*) were measured after 1, 5, and 10 sec depolarizations from -90 mV to the voltage of peak current. Asterisks indicate statistically significant difference (*$p < 0.05$; **$p < 0.01$; unpaired Student's *t* test).

tsA-201 cells (I_{Ba} current density, BayK absent, 0.86 $\pm$ 0.089 pA/pF, $n = 10$; BayK present, 17.6 $\pm$ 9.2 pA/pF, $n = 6$). For I_{Ca}, but not I_{Ba}, a small but significant 4.8 mV shift of $V_{0.5,act}$ to more negative potentials was evident in *X. laevis* oocytes ($p < 0.001$) (Table 1). This significant difference remained when subgroups with different current amplitudes (0.30–0.59 vs 0.60–1.0 μA) were compared (data not shown). The amplitudes of I_{Ba} and I_{Ca} recorded in the same oocyte were similar (Table 1), indicating that this mutation also affects divalent cation permeability. For Ba^{2+} currents, the inactivation time course was significantly faster than for WT ($p < 0.001$), with 57.7 $\pm$ 2.1% ($n = 18$) inactivating during 10 sec pulses (Fig. 3*A,B*). In contrast to I_{Ba}, I_{Ca} inactivation of LP was similar to WT at the end of the 10 sec depolarizing pulse, and LP even slowed the early phase of I_{Ca} inactivation (Fig. 3*D*).
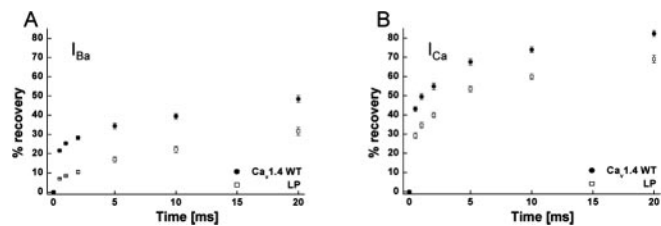

Figure 4. Recovery of inactivation of Ca$_v$1.4 WT and mutant LP α1 subunits. The percentage of recovery from the inactivated current was determined after 0.5, 1, 2, 5, 10, and 20 sec after a 10 sec depolarization to V_{max} plus 10 mV for Ca$_v$1.4 WT and mutant LP α1 subunits coexpressed with β3 and α2δ1 subunits in *X. laevis* oocytes. A concentration of 10 mM Ba^{2+} (*A*) or 10 mM Ca^{2+} (*B*) was used as charge carriers (10 μM of BayK present). The extent of recovery was statistically significant after all of the time points indicated for I_{Ba} and I_{Ca} compared with WT ($p < 0.001$; unpaired Student's *t* test).
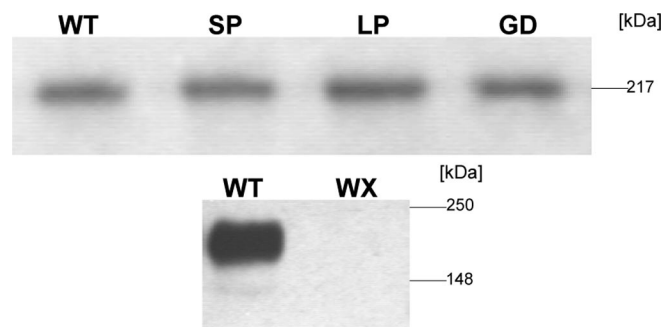

Figure 5. Heterologous expression of Ca$_v$1.4 WT and different mutant α1 subunits in tsA-201 cells. Human embryonic kidney tsA201 cells were transfected with Ca$_v$1.4 WT and mutant GD, LP, SP, and WX α1 subunits together with β3 and α2δ1 subunit cDNAs, as described in Materials and Methods. Ca$_v$1.4 α1 subunit proteins were quantified in immunoblots of microsomal membranes prepared from lysed cells after separation on 8% SDS-PAGE gels (10 μg of membrane protein per lane) using a generic anti-α1 sequence-directed antibody (anti-Ca$_v$1.1 α1-1382-1400). Ca$_v$1.4 WT and mutants migrated with the expected molecular weight of 219 kDa. Staining was absent for the WX mutant (calculated molecular weight of 161 kDa). One representative of three experiments yielding similar results is shown.

Stable recordings of Ca$_v$1.4-mediated currents were possible over long time periods in oocytes and allowed us to investigate changes of the recovery from inactivation of mutant LP. Note that, because of its very slow inactivation time course, these measurements were not feasible for GD. WT and LP channels were inactivated by 10 sec depolarizing pulses to V_{max} and then allowed to recover for various time periods before short test pulses to V_{max} were applied to quantify current recovery. Figure 4 illustrates that, in WT channels, 80% of I_{Ca} (Fig. 4*B*) recovered within 20 sec, but only ~50% of I_{Ba} recovered within 20 sec (Fig. 4*A*). Mutation LP significantly slowed recovery with both charge carriers (percentage of recovering current; I_{Ba}: WT, 48.4 $\pm$ 1.8%, $n = 9$; LP, 31.6 $\pm$ 2.1%, $n = 6$; $p < 0.001$; I_{Ca}: WT, 82.4 $\pm$ 1.5%, $n = 8$; LP, 69.1 $\pm$ 2.0%, $n = 7$; $p < 0.001$).

Because mutants SP and WX did not form functional channels, we investigated the possibility that they reduce expression of the α1 subunit protein. To test this possibility, we transfected tsA-201 cells with all of the mutant constructs and WT together with α2δ1 and β3 subunits and measured the expression of α1 protein in Western blots (Fig. 5). No WX α1 protein could be detected, although the epitope of the antibody at the beginning of the C-terminal tail was preserved in this mutant, and cDNA integrity was confirmed by DNA sequencing (see Materials and Methods). In contrast, SP α1 expression was indistinguishable

from WT, indicating that this mutation does not generally prevent α1 expression. Mutations GD and LP also caused no detectable change in α1 subunit expression.

Discussion

Although it is widely accepted that disease symptoms of CSNB2 result from a complete loss of Ca$_v$1.4 channel function, it remains unclear to which extent channel function must be compromised. Our study therefore focused on structural aberrations still likely to support Ca^{2+} channel activity. We found that three CSNB2 missense mutations either caused profound changes of Ca$_v$1.4 gating or completely prevented channel function. We also report for the first time that the disease can be caused by a mutation (GD) with characteristics that should result in a gain of LTCC function.

GD shifted the voltage dependence of activation to more negative voltages independent of the charge carrier, slowed activation and inactivation kinetics, and removed CDI. All changes should promote Ca^{2+} entry through the channel. This raises the important question about how increased channel function could impair light-induced signaling between photoreceptors and second-order neurons. In the dark, photoreceptors depolarize to a resting membrane potential of -36 to -40 mV (Corey et al., 1984; Witkovsky et al., 1997; Schneeweis and Schnapf, 2000; Moriondo et al., 2001), inducing tonic glutamate release. The latter is linearly related to cytoplasmic Ca^{2+} concentrations and LTCC activity (Witkovsky et al., 1997). Light absorption in the photoreceptor outer segments and closure of cGMP-gated cation channels hyperpolarizes the cells to below -55 mV (Witkovsky et al., 1997). Because the $V_{0.5,act}$ for retinal L-type channels (and Ca$_v$1.4) (Koschak et al., 2003; McRory et al., 2004) is clearly above -40 mV (Corey et al., 1984; Wilkinson and Barnes, 1996), the retinal operating range of membrane potential changes is at the "foot" of the LTCC I–V curve, and thus Ca^{2+} influx becomes very small or unmeasurable (Witkovsky et al., 1997) at hyperpolarized voltages maintained during illumination. The pronounced negative shift of the activation curve by the GD mutation must result in a significant increase of Ca^{2+} influx during illumination. Assuming a $V_{0.5,act}$ of -22 mV and a slope of 4.3 mV for the I–V curve (values measured for retinal Ca^{2+} channels at physiological Ca^{2+} concentrations that are close to the parameters found in this study) (Corey et al., 1984), a sigmoidal Boltzmann equation can be used to calculate I_{Ca} to amount to 4.6% of maximal current in the dark (-35 mV) and to 0.04% during illumination (-55 mV). This corresponds to a 100-fold decrease of I_{Ca} during light exposure. Assuming a shift of $V_{0.5,act}$ by the GD mutation by -20 mV for I_{Ca} (Table 1), 83% of I_{Ca} would be active in the dark and 4.6% during illumination, corresponding to an 18-fold decrease. Therefore, the GD mutation would result in an overall increase of Ca^{2+} entry but at the same time would reduce the dynamic range by almost sixfold. An equivalent change in the dynamic range of tonic glutamate release could then explain how the synaptic gain between first- and second-order neurons is reduced by this mutation.

Our data confirm existing models on the role of S6 segments for channel inactivation and extend them to Ca$_v$1.4. Slowing of inactivation by the GD mutation fits with the hypothesis that residues in the pore-lining S6 segments and especially those at their cytoplasmic ends are crucial determinants of slow Ca^{2+} channel inactivation. GD is located next to a serine residue (Fig. 1) found previously to contribute to the formation of an annular structure on the cytoplasmic end of the channel, which may constrict the cytoplasmic pore opening during inactivation (Shi and

Soldatov, 2002) and/or may serve as a receptor for a gating particle formed by the I–II linker (Stotz et al., 2004). Mutations in the S6 region have also been shown to eliminate CDI of Ca$_v$1.2 LTCCs (Shi and Soldatov, 2002). We also found that GD contributes to CDI in Ca$_v$1.4. This mutation also shifts $V_{0.5,act}$ and affects ion selectivity, suggesting that the negative charge introduced by the GD mutation at the cytoplasmic side of IS6 cannot only affect conformational changes associated with channel activation but can also interfere with cation permeation through the proposed cytoplasmic end of the pore.

Both other missense mutations and the WX truncation induced changes compatible with a loss of function. For LP, we could only record significant currents in the presence of BayK, independent of the expression system used. BayK triggered the appearance of robust L-type currents comparable with WT. Because BayK cannot rapidly recruit channels to the plasma membrane, this may best be explained by a mutation-induced reduction of open probability overcome by BayK. Interestingly, the mutated leucine 1068 is located next to phenylalanine 1069 and very close to serine 1072 (Fig. 1), which were both found to play a critical role for the action of dihydropyridine (DHP) channel activators (Yamaguchi et al., 2003). The LP mutation may thus stabilize a pore conformation that inhibits channel opening. As a result of the low-expression efficiency (see above), single-channel measurements of Ca$_v$1.4 channels are difficult. Therefore, future experiments should determine whether mutations of this leucine residue also cause similar changes in other LTCCs more easily accessible to single-channel analysis. The observation that LP supports channel activity in the presence of BayK also has potential therapeutic implications, because Ca$_v$1.4 activators may restore activity and improve CSNB2 symptoms. In the case of LP, a complete drug-induced recovery of function is, however, unlikely because of the other gating changes found in our study. For example, LP also significantly slowed the recovery from inactivation, which would favor a decrease in I_{Ca} caused by the accumulation of channels in inactivated states during cycling between hyperpolarized and depolarized membrane potentials.

Mutations SP and WX did not support Ca^{2+} channel activity. For WX, this can be explained by the failure to express α1 protein, which is evident from transfected tsA-201 cells. This indicates an important role of the C-terminal tail for proper Ca$_v$1.4 protein processing and targeting.

The SP mutation did not reduce α1 protein expression in tsA-201 cells, suggesting that loss of function does not result from an overall failure of α1 protein synthesis. Although it remains to be determined why this mutant fails to support Ca^{2+} channel activity in oocytes, it is likely that it either prevents α1 subunit targeting to the plasma membrane or obstructs channel gating. The failure of SP to support channel activity emphasizes the important role of this residue for voltage-gated Ca^{2+} channel function. Accordingly, a mutation of this conserved serine residue in Ca$_v$2.1 channels also results in human pathology (severe forms of FHM1) (Kors et al., 2001).

Our data for GD and WX differ from a previous report (McRory et al., 2004) in which neither the pronounced negative shift of the I–V curve nor changes in inactivation were observed. Only a minimal (but statistically significant) change in the slope of activation and a less pronounced shift of the half-activation potential to more positive voltages with Ca^{2+} compared with Ba^{2+} as charge carrier were found. We ruled out the idea that differences in the expression system account for this discrepancy. McRory et al. (2004) also found normal current amplitudes and

gating kinetics for mutant WX. One possible explanation is the structural differences in the Ca$_v$1.4 α1 subunits used to study the mutations. The construct used by McRory et al. (2004) differs from ours in four positions (K vs R in position 58, E vs G in position 380, R vs H in position 1282, and I vs V in position 1306). These residues are highly conserved among LTCCs and non-LTCCs (alignments not shown) and may represent so far unknown [National Center for Biotechnology Information (NCBI) GenBank and Ensembl databases] polymorphisms of *CACNA1F*. Interestingly, the G369D mutation affects a glycine residue localized in a very conserved region at the cytoplasmic end of IS6 and introduces a negative charge. As mentioned previously, the construct used by McRory et al. (2004) contains a glycine residue replacing a glutamate residue at position 380. The absence of this negative charge close to the G369D mutation may prevent an electrostatic interaction between the D369 and the E380 residue, which can occur in our mutant GD but not in McRory's mutant GD construct nor in their, or our, WT Ca$_v$1.4 α1. It will therefore be interesting to test in future experiments whether this electrostatic interaction can indeed affect channel gating. In addition, their construct represents a different splice variant and contains an 11 amino acid insertion in the I–II linker and a seven amino acid deletion in the domain IVS3–IVS4. Additional experiments must also test the interesting possibility that alternative splicing or single-nucleotide polymorphisms can affect the phenotype of CSNB2 mutations.

McRory et al. (2004) also analyzed mutants G674D and A928D (G663D and A917D in our Ca$_v$1.4 α1 construct) and found no evidence for gating changes in tsA-201 cells. Similarly, we found no gating changes for mutations R508Q and L1368H, but both caused a decrease of α1 subunit synthesis in tsA-201 cells ($n = 3$; data not shown). We are currently investigating the consequences of decreased protein expression on current density in different expression systems.

Ca$_v$1.4 α1 subunits also occur in immune cells, such as in mast and plasma cells (McRory et al., 2004). Based on our findings, immune cells from patients carrying the CSNB2 mutations analyzed here may provide novel probes to study the role of Ca$_v$1.4 in the human immune system.

References

Ball SL, Powers PA, Shin HS, Morgans CW, Peachey NS, Gregg RG (2002) Role of the β2 subunit of voltage-dependent calcium channels in the retinal outer plexiform layer. Invest Ophthalmol Vis Sci 43:1595–1603.

Barnes S, Kelly ME (2002) Calcium channels at the photoreceptor synapse. Adv Exp Med Biol 514:465–476.

Baumann L, Gerstner A, Zong X, Biel M, Wahl-Schott C (2004) Functional characterization of the L-type Ca^{2+} channel Ca$_v$1.4 α1 from mouse retina. Invest Ophthalmol Vis Sci 45:708–713.

Bech-Hansen NT, Naylor MJ, Maybaum TA, Pearce WG, Koop B, Fishman GA, Mets M, Musarella MA, Boycott KM (1998) Loss-of-function mutations in a calcium-channel α1-subunit gene in Xp11.23 cause incomplete X-linked congenital stationary night blindness. Nat Genet 19:264–267.

Boycott KM, Pearce WG, Bech-Hansen NT (2000) Clinical variability among patients with incomplete X-linked congenital stationary night blindness and a founder mutation in CACNA1F. Can J Ophthalmol 35:204–213.

Castellano A, Wei X, Birnbaumer L, Perez-Reyes E (1993) Cloning and expression of a third calcium channel β subunit. J Biol Chem 268:3450–3455.

Catterall WA (2000) Structure and regulation of voltage-gated Ca^{2+} channels. Annu Rev Cell Dev Biol 16:521–555.

Corey DP, Dubinsky JM, Schwartz EA (1984) The calcium current in inner segments of rods from the salamander (*Ambystoma tigrinum*) retina. J Physiol (Lond) 354:557–575.

Ellis SB, Williams ME, Ways NR, Brenner R, Sharp AH, Leung AT, Campbell KP, McKenna E, Koch WJ, Hui A, Schwartz A, Harpold MM (1988) Sequence and expression of mRNAs encoding the α1 and α2 subunits of a DHP-sensitive calcium channel. Science 241:1661–1664.

Hess P, Lansman JB, Tsien RW (1986) Calcium channel selectivity for divalent and monovalent cations. Voltage and concentration dependence of single channel current in ventricular heart cells. J Gen Physiol 88:293–319.

Horton RM, Hunt HD, Ho SN, Pullen JK, Pease LR (1989) Engineering hybrid genes without the use of restriction enzymes: gene splicing by overlap extension. Gene 77:61–68.

Huber I, Wappl E, Herzog A, Mitterdorfer J, Glossmann H, Langer T, Striessnig J (2000) Conserved Ca^{2+} antagonist binding properties and putative folding structure of a recombinant high affinity dihydropyridine binding domain. Biochem J 347:829–836.

Kors EE, Terwindt GM, Vermeulen FL, Fitzsimons RB, Jardine PE, Heywood P, Love S, van den Maagdenberg AM, Haan J, Frants RR, Ferrari MD (2001) Delayed cerebral edema and fatal coma after minor head trauma: role of the CACNA1A calcium channel subunit gene and relationship with familial hemiplegic migraine. Ann Neurol 49:753–760.

Koschak A, Reimer D, Walter D, Hoda JC, Heinzle T, Grabner M, Striessnig J (2003) Ca$_v$1.4 α1 subunits can form slowly inactivating dihydropyridine-sensitive L-type Ca^{2+} channels lacking Ca^{2+}-dependent inactivation. J Neurosci 23:6041–6049.

Krieg PA, Melton DA (1984) Functional messenger RNAs are produced by SP6 *in vitro* transcription of cloned cDNAs. Nucleic Acids Res 12:7057–7070.

Liang H, DeMaria CD, Erickson MG, Mori MX, Alseikhan BA, Yue DT (2003) Unified mechanisms of Ca^{2+} regulation across the Ca^{2+} channel family. Neuron 39:951–960.

McRory JE, Hamid J, Doering CJ, Garcia E, Parker R, Hamming K, Chen L, Hildebrand M, Beedle AM, Feldcamp L, Zamponi GW, Snutch TP (2004) The CACNA1F gene encodes an L-type calcium channel with unique biophysical properties and tissue distribution. J Neurosci 24:1707–1718.

Morgans CW (2000) Neurotransmitter release at ribbon synapses in the retina. Immunol Cell Biol 78:442–446.

Morgans CW, Gaughwin P, Maleszka R (2001) Expression of the α1F calcium channel subunit by photoreceptors in the rat retina. Mol Vis 7:202–209.

Moriondo A, Pelucchi B, Rispoli G (2001) Calcium-activated potassium current clamps the dark potential of vertebrate rods. Eur J Neurosci 14:19–26.

Murakami M, Nakagawasai O, Fujii S, Kameyama K, Murakami S, Hozumi S, Esashi A, Taniguchi R, Yanagisawa T, Tan-no K, Tadano T, Kitamura K, Kisara K (2001) Antinociceptive action of amlodipine blocking N-type Ca^{2+} channels at the primary afferent neurons in mice. Eur J Pharmacol 419:175–181.

Perez-Reyes E, Castellano A, Kim HS, Bertrand P, Baggstrom E, Lacerda AE, Wei X, Birnbaumer L (1992) Cloning and expression of a cardiac/brain β subunit of the L-type calcium channel. J Biol Chem 267:1792–1797.

Platzer J, Engel J, Schrott-Fischer A, Stephan K, Bova S, Chen H, Zheng H, Striessnig J (2000) Congenital deafness and sinoatrial node dysfunction in mice lacking class D L-type calcium channels. Cell 102:89–97.

Safayhi H, Haase H, Kramer U, Bihlmayer A, Roenfeldt M, Ammon HP, Froschmayr M, Cassidy TN, Morano I, Ahlijanian M, Striessnig J (1997) L-type calcium channels in insulin-secreting cells: biochemical characterization and phosphorylation in RINm5F cells. Mol Endocrinol 11:619–629.

Schneeweis DM, Schnapf JL (2000) Noise and light adaptation in rods of the macaque monkey. Vis Neurosci 17:659–666.

Shi C, Soldatov NM (2002) Molecular determinants of voltage-dependent slow inactivation of the Ca^{2+} channel. J Biol Chem 277:6813–6821.

Splawski I, Timothy KW, Sharpe LM, Decher N, Kumar P, Bloise R, Napolitano C, Schwartz PJ, Joseph RM, Condouris K, Tager-Flusberg H, Priori SG, Sanguinetti MC, Keating MT (2004) Ca$_v$1.2 calcium channel dysfunction causes a multisystem disorder including arrhythmia and autism. Cell 119:19–31.

Stotz SC, Jarvis SE, Zamponi GW (2004) Functional roles of cytoplasmic loops and pore lining transmembrane helices in the voltage-dependent inactivation of HVA calcium channels. J Physiol (Lond) 554:263–273.

Strom TM, Nyakatura G, Apfelstedt-Sylla E, Hellebrand H, Lorenz B, Weber

BH, Wutz K, Gutwillinger N, Ruther K, Drescher B, Sauer C, Zrenner E, Meitinger T, Rosenthal A, Meindl A (1998) An L-type calcium-channel gene mutated in incomplete X-linked congenital stationary night blindness. Nat Genet 19:260–263.

Tremblay F, Laroche RG, De Becker I (1995) The electroretinographic diagnosis of the incomplete form of congenital stationary night blindness. Vision Res 35:2383–2393.

Wheeler DB, Tsien RW, Randall A (1994) Identification of calcium channels that control neurosecretion. Science 266:828–831.

Wilkinson MF, Barnes S (1996) The dihydropyridine-sensitive calcium channel subtype in cone photoreceptors. J Gen Physiol 107:621–630.

Witkovsky P, Schmitz Y, Akopian A, Krizaj D, Tranchina D (1997) Gain of rod to horizontal cell synaptic transfer: relation to glutamate release and a dihydropyridine-sensitive calcium current. J Neurosci 17:7297–7306.

Yamaguchi S, Zhorov BS, Yoshioka K, Nagao T, Ichijo H, Adachi-Akahane S (2003) Key roles of Phe1112 and Ser1115 in the pore-forming IIIS5–S6 linker of L-type Ca^{2+} channel α1C subunit (Ca$_v$ 1.2) in binding of dihydropyridines and action of Ca^{2+} channel agonists. Mol Pharmacol 64:235–248.

Yang J, Ellinor PT, Sather WA, Zhang JF, Tsien RW (1993) Molecular determinants of Ca^{2+} selectivity and ion permeation in L-type Ca^{2+} channels. Nature 366:158–161.

Zamponi GW (2003) Regulation of presynaptic calcium channels by synaptic proteins. J Pharmacol Sci 92:79–83.